Catalysis Today 155 (2010) 157–163

Contents lists available at ScienceDirect

Catalysis Today

journal homepage: www.elsevier.com/locate/cattod

MRI: *Operando* measurements of temperature, hydrodynamics and local reaction rate in a heterogeneous catalytic reactor

Lynn F. Gladden *, Fernando J.R. Abegão, Christopher P. Dunckley, Daniel J. Holland, Mark H. Sankey, Andrew J. Sederman

University of Cambridge, Department of Chemical Engineering and Biotechnology, Pembroke Street, Cambridge CB2 3RA, United Kingdom

ARTICLE INFO

Article history:
Available online 20 November 2009

Keywords:
Magnetic resonance
Trickle-bed reactor
Temperature
Velocity
Concentration

ABSTRACT

Magnetic resonance imaging is a particularly valuable technique for studying heterogeneous catalytic processes in the reactor environment because it has the potential to characterise hydrodynamics and chemical composition at different spatial locations within the reactor. Here we report recent developments in: (i) temperature mapping in a trickle-bed reactor with an accuracy of ±2.0 °C, (ii) imaging of local gas and liquid flow velocities in a fixed-bed reactor during trickle-flow with a measurement accuracy of 5% and 7%, respectively, and (iii) quantitative mapping of chemical composition within the bed to an accuracy of <2.5%. The ability to measure local reaction rate enables us to calculate a local rate-based selectivity to specific products within the reactor.

1. Introduction

Designing and optimising the operation of trickle-bed reactors (TBRs) presents a long-standing challenge in catalytic reactor engineering. TBRs consist of a column that may be 10–30 m in height packed with a fixed-bed of catalyst. Typically a gas–liquid feed is introduced to the column co-currently downwards. The gas and liquid are supplied to the packing at flow rates such that the spatial distribution of the gas and liquid remains constant with time; i.e., we are operating in the trickle-flow regime. Examples of operations carried out in TBRs in this mode of operation include hydrodesulphurization, hydrodemetallization, hydrocracking and hydrotreating [1]. In 1992, Gianetto and Specchia [1] presented an overview of the information that is required to model reactor performance. Such information includes: (i) the extent of fluid solid contacting, (ii) the hydrodynamic regime in which the catalyst is operating, (iii) the extent of axial dispersion within the reactor, (iv) mass transfer between gas and liquid phases, (v) concentration gradients between the inter- and intra-particle space of the reactor, (vi) catalyst wetting efficiency, (vii) liquid hold-up, and (viii) temperature variations within the bed. Many of these data are difficult to access using conventional measurement techniques. Magnetic resonance techniques are particularly well-suited to *operando* studies of catalytic process environments because of their ability to measure chemical composition and transport processes (diffusion and flow) within three-dimensional, optically opaque systems [2,3]. In applying magnetic resonance imaging (MRI) techniques to study catalytic reactors we have the ability to characterise reactor, and hence catalyst performance, at a local level within the reactor. This is important because the activity and selectivity associated with a given catalyst pellet within the reactor is likely to be influenced by the boundary conditions (i.e., catalyst wetting, flow field adjacent to the catalyst surface) under which it operates. The development and application of *operando* MRI techniques therefore have the potential to aid the integrated design and operation of catalyst and fixed-bed catalytic reactor. It is worth noting that whilst the reactor studied by MRI is considerably smaller than that used in industrial practice, scale-up from beds of the size used in the MRI experiment is accepted procedure and therefore the results obtained from these MRI studies are relevant to industrial operation.

There now exist numerous examples of MRI applied to heterogeneous catalytic reactors. These include quantification of catalyst wetting (liquid–solid contacting) and hold-up [4,5], imaging of single-phase liquid flow fields [6], characterisation of hydrodynamic transitions in reactors [7], and spatial mapping of chemical composition [8–11] within reactors. In this paper results of three ongoing studies are reported which add to the portfolio of measurements that can be undertaken using *operando* MRI measurements. All the experiments were conducted within a 4.7 T super-wide bore superconducting magnet linked to a Bruker Biospin DMX200 spectrometer. First, the principles behind a simple measurement of temperature mapping within a reactor are described and an example is given. Second, the ability to measure not only liquid velocity within the reactor but also gas velocity is demonstrated. Finally, recent developments in the quantification

* Corresponding author. Tel.: +44 1223 334762.
E-mail address: Gladden@cheng.cam.ac.uk (L.F. Gladden).

0920-5861/$ – see front matter © 2009 Elsevier B.V. All rights reserved.
doi:10.1016/j.cattod.2009.10.012

of spatially resolved measurements of chemical composition are summarized. The 1-octene hydrogenation reaction was used for both the temperature and chemical composition studies because it is a fast and exothermic reaction at moderate temperatures and pressures, thus a significant conversion is achieved in a single pass through the reactor.

2. Temperature mapping

The performance of fixed-bed reactors often shows high sensitivity to operating temperature and to temperature gradients within the catalyst bed. Conversion, selectivity, thermal stability and catalyst lifetime can all be highly sensitive to temperature. MRI has been used to measure temperature using a number of approaches, e.g. signal intensity, relaxation times, diffusivities, and chemical shift variation [12]. Such methods are preferable to a thermocouple as they are less invasive and, in contrast to metallic probes, do not spoil images acquired with other MRI methods. Temperature mapping in a catalytic reactor has previously been reported using measurements of ^{27}Al signal intensity [13]. In the present work, we study the temperature within a TBR during 1-octene hydrogenation by measuring the chemical shift variation of ethylene glycol contained in glass microspheres using volume selective spectroscopy (VOSY) [14]. The chemical shift approach used is robust to magnetic susceptibility differences between the gas, liquid and solid phases in the reactor, and can measure temperature with an accuracy that is comparable to that of a thermocouple. For temperatures between 25 and 110 °C, the chemical shift ($\Delta\delta$) between the –OH and the –CH_2 spectral peaks of ethylene glycol is well documented in the literature [15]. Not only does this method have the advantage of covering a wide temperature range but also it does not need an external reference since the chemical shifts are relative chemical shifts for different groups in the same compound. It is this aspect of the measurement which gives the measurement its robustness, by avoiding artefacts related to magnetic field inhomogeneities and differences in temperature between the 'thermometer' compound and any reference compound.

A glass reactor (inner diameter 25 mm) was packed with 2 wt% Pd/Al_2O_3 catalyst trilobes (2 mm diameter, 6 ± 2 mm length) to form a bed of ~30 mm length. The catalyst was surrounded above and below by 30 mm layers of pure Al_2O_3 trilobes to provide enhanced gas–liquid distribution and support, respectively. Four spherical bulb inserts (18 μl, outer diameter 4 mm) were filled with anhydrous ethylene glycol (99.8%) and placed within the catalyst bed. The catalyst was reduced in a 20:80 (v/v). % hydrogen:nitrogen gas flow for 1.5 h prior to study. The reaction was initiated by introducing a feed of 1-octene at a flow rate of 0.05 ml s^{-1} along with a gas mixture of H_2:N_2 (in a 20:80, v/v%) at a flow rate of 3.1 ml s^{-1} and 1 barg. The reactants were introduced at ambient temperature (20 °C) and air was passed over the reactor to prevent over-heating of the radio-frequency (r.f.) coil. After 2 h of reaction, the liquid flow rate was increased to 0.08 ml s^{-1} to reduce the temperature of the reactor and hence control hot-spot formation. The reactor was operated in the trickle-flow regime at all times. Analysis of the exit stream by GC showed an overall conversion of 1-octene of ~18%, with a selectivity to octane of ~43%.

Various images were acquired using the Rapid Acquisition with Relaxation Enhancement (RARE) pulse sequence [16]. RARE is one of a number of fast MR imaging pulse sequences; these have been discussed in greater detail elsewhere [2]. The basic principle of this fast imaging approach requires the concept of the **k**-space raster; the time domain data acquired in the MR experiment can be thought of as a two-dimensional (2D) rectilinear array (if a 2D image is being obtained) in **k**-space. In conventional MRI a new r.f. excitation is required to read each line of **k**-space—this means that typical imaging times are orders of several minutes. In the RARE approach, multiple lines of **k**-space are acquired from a single r.f. excitation. Often the entire 2D **k**-space array is acquired (i.e., the whole image) from a single r.f. excitation, yielding image acquisition times of 100–500 ms. The number of lines of **k**-space acquired from each excitation is referred to as the RARE factor. RARE is particularly useful here since it is particularly robust (i.e., artefact free), and far more robust than other fast MR techniques, in application to systems characterised by heterogeneous magnetic susceptibility typical of those found in reaction engineering. In the context of the present paper, the RARE imaging technique is used to provide an image of liquid distribution within the bed. If greater accuracy in this liquid distribution is required, greater signal averaging is performed. All images used in this study had total acquisition times of less than 150 s, even for multi-slice image acquisitions. Prior to reactor start-up, multi-slice RARE images in the transverse and in the longitudinal planes were acquired to visualise the structure of the bed and to serve as reference images to aid the positioning of the cubic voxels in the VOSY experiments. Eight image slices were acquired in each multi-slice RARE experiment. Each of the longitudinal slices had a field-of-view (FOV) of 50 mm (z) × 36.7 mm (x) and was acquired with an in-plane resolution of 390 μm (z) × 287 μm (x). For the transverse slices the FOV was 36.7 mm × 36.7 mm and the in-plane resolution was 286 μm (x) × 286 μm (y). These multi-slice acquisitions were also employed to study the liquid distribution in the reactor during start-up; typical acquisition times were ~30 s.

The ethylene glycol thermometer was calibrated in an independent experiment in which a hot air stream was passed through an insulated PEEK cell within which the glass bulb containing ethylene glycol was placed. The temperature of the air stream was monitored using a thermocouple and was varied between 25 and 110 °C. Thermal equilibrium was achieved prior to measurement of the calibration spectra. Over the range of temperatures studied, the data were well described by a linear relationship of the form:

$$T(^\circ\mathrm{C}) = -100.5(\pm 0.8) \times |\Delta\delta| + 191.6(\pm 1.1). \quad (1)$$

In the present experiments it was possible to achieve an accuracy of 0.003 ppm in the determination of chemical shift, and therefore the temperature could be measured to an accuracy of ±1.4 °C. Eq. (1) is in agreement with previous correlations between ethylene glycol chemical shift and temperature reported in the literature [17–19]. The measurement was then performed in the trickle-bed reactor in which the 1-octene hydrogenation was occurring. The chemical shift was measured using a spin-echo VOSY pulse sequence to isolate the signal within a cubic voxel of 2 mm side length. Spectral data were acquired with 8 scans during reactor start-up and 32 scans during steady state operation, corresponding to a total acquisition time of 24 and 96 s, respectively. In both cases the echo time and recycle delay were 1.86 ms and 3 s, respectively. Reference measurements were carried out in a TBR in which no reaction was occurring; in this case, temperature measurements were acquired using both a thermocouple and MRI simultaneously. In these studies, both methods were in agreement to within ±0.6 °C. For the TBR in which reaction was occurring, errors were estimated to be within ± 2 °C.

Fig. 1 shows typical data acquired in the MRI and VOSY experiments. Fig. 1a shows a RARE MRI image. Signal intensity is associated with the presence of liquid. Under these operating conditions there is relatively little inter-particle liquid, and signal intensity is seen arising primarily from liquid in the internal pore space of the catalyst pellets. In this particular image a hot-spot is observed; in the region of the hot-spot a loss of signal is observed since the MRI experiment is not sensitive to signal from species in the vapour phase. It is noted that before hydrogen was introduced

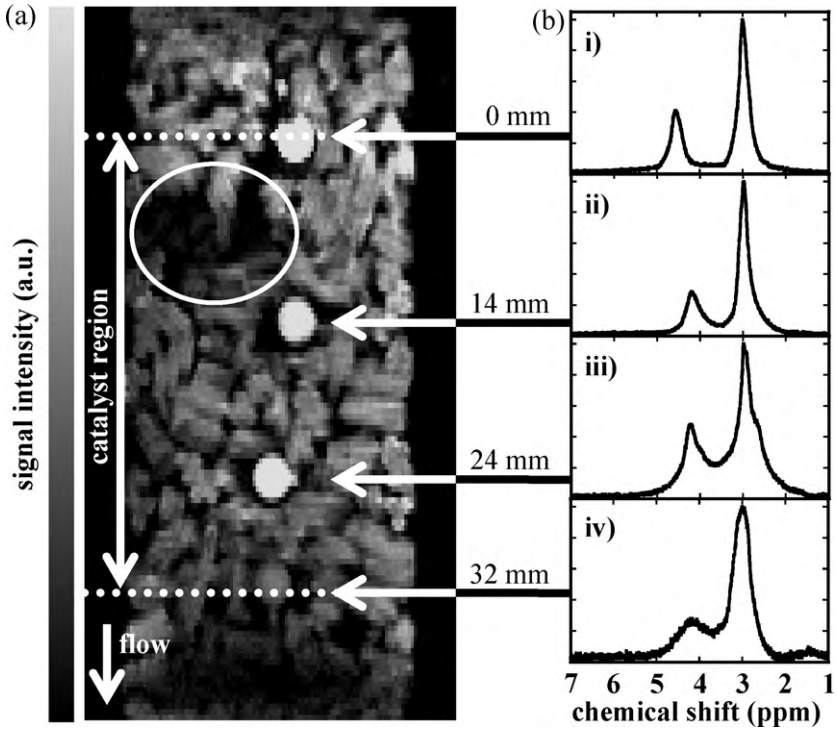

Fig. 1. Temperature measurements during 1-octene hydrogenation over a 2 wt% Pd/Al_2O_3 catalyst. (a) RARE MRI image showing the position of the 4 glass microspheres containing ethylene glycol. The field-of-view was 50 mm (z) × 36.7 mm (x) and the spatial resolution was 390 μm (z) × 287 μm (x). The data were acquired with a RARE factor of 16, an echo time of 2.51 ms and a recycle delay of 1.0 s. The image was acquired by averaging 16 scans, giving a total image acquisition time of 132 s. The dotted lines indicate the beginning and the end of the catalyst region. The liquid-free region in the bed, which we have identified as a region of hot-spot formation, is highlighted. (b) NMR spectra of ethylene glycol contained in the microspheres acquired with the VOSY pulse sequence at (i) 0 mm, (ii) 14 mm, (iii) 24 mm and (iv) 32 mm.

this region of signal loss was not observed. In Fig. 1, the 4 glass microspheres containing ethylene glycol are positioned at the vertical positions identified as 0, 14, 24 and 32 mm. The microsphere located at 32 mm has a low signal intensity. This is because it is positioned towards the edge of the imaging coil where the coil response and therefore signal-to-noise ratio of the measurement is lower. Fig. 1b shows the spectra recorded after 400 min on stream. Under these conditions the reactor is operating at steady state although temperature oscillations can still be observed, and are primarily associated with hot-spot formation. These observations will be discussed in detail in a future publication. Note that the VOSY spectrum reported at 32 mm is noisier than the other 3 spectra shown; this results from this microsphere being positioned at the edge of the imaging coil as stated earlier. However, the signal-to-noise in this spectrum is still sufficiently good that the chemical shift difference between the peaks in the spectrum can be measured and therefore the temperature measurement is still of similar accuracy as that from the other "temperature sensor" microspheres. From the data shown in Fig. 1b it is seen that the chemical shift difference between the peaks narrows significantly between the microspheres located at 0 and 14 mm. Further down the bed the peak separation differs very little. At 0 mm, the peak separation is 1.52 ppm corresponding to (from Eq. (1)) a local temperature measurement of 39 °C. At 14 mm, the peak separation has reduced to 1.21 ppm, indicating a temperature of 70 °C. Fig. 2 shows the evolution of temperature at the locations shown in Fig. 1a, as a function of time-on-stream from start-up of the reactor.

3. Imaging gas and liquid velocity fields

Heat and mass transfer in trickle-bed reactors are strongly influenced by the local distribution and velocity of the gas and liquid contained in them. Previous MRI studies of two-phase flow in fixed-bed reactors have been limited to observations of the liquid distribution [4,20]. These measurements have now been extended to image not just the distribution of liquid and gas within the reactor but the velocity with which the liquid and gas are moving. The primary motivation for developing this measurement capability is to be able to measure adjacent gas and liquid velocity fields within the reactor. This will give insight to the likely heterogeneity of gas–liquid mass transfer processes within the

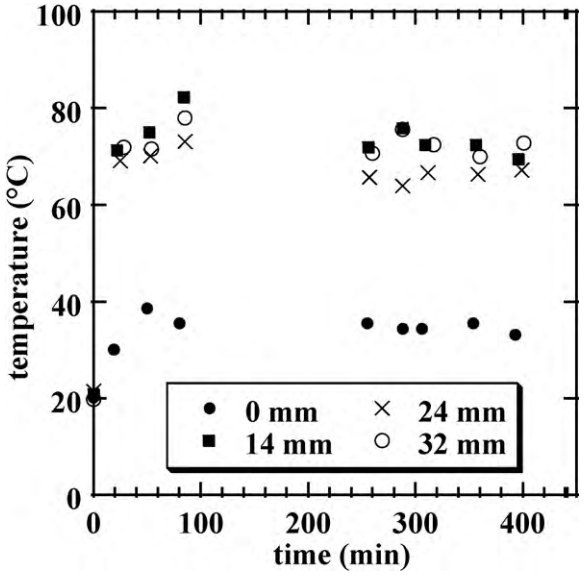

Fig. 2. Evolution of the temperature in each of the microspheres shown in Fig. 1a during reactor start-up.

reactor as well as providing input to the use of appropriate closure laws in computational fluid dynamics simulations. Of course, the measured velocity fields also enable direct evaluation of the ability of numerical simulation codes to predict the characteristics of two-phase flow in reactor environments. In the example given here, the gas–liquid flow is occurring within a non-reacting medium. However, the measurement technique is readily transferable to a packing of catalyst, as opposed to glass spheres, and to operating conditions under which reaction is occurring. Imaging of hydrocarbon gases does represent an additional challenge because of less favourable relaxation times and the high intensity ^{1}H signal associated with the liquid phase; however, these problems are not insurmountable and this is the subject of ongoing work.

To achieve gas velocity measurements, SF_6 gas has been used because it has particularly favourable MR characteristics. In addition to the high gyromagnetic ratio of ^{19}F and the large number of ^{19}F nuclei per molecule, SF_6 has a relatively low self-diffusion coefficient; a low self-diffusion coefficient reduces diffusive attenuation in the presence of magnetic field gradients, and also reduces diffusive blurring, thereby improving image resolution. Further, SF_6 has short relaxation times which allows many signal-averages per unit time, thereby improving the signal-to-noise ratio. However, low values of spin–spin relaxation time make it difficult to implement velocity measurements for moderate velocities, say $<1\ m\ s^{-1}$, because of the limit to the maximum value of the observation time that can be employed. We have therefore used a strategy in which SF_6 is pressurised; this has three benefits. First, it increases the spin density in direct proportion to the pressure, thereby enhancing MR sensitivity. Second, the molecular self-diffusion coefficient decreases in inverse proportion to pressure; this reduces diffusive attenuation and blurring. Third, the relaxation times of ^{19}F in SF_6 increase approximately linearly with pressure; this allows the successful implementation of spin-echo velocity imaging pulse sequences capable of measuring velocities down to $\sim 10\ mm\ s^{-1}$.

The technique development associated with this work and a full description of the experimental procedure was recently reported by Sankey et al. [21]. In summary, gas and liquid were flowed co-currently downwards through a bed of sodalime glass spheres with diameter 5.0 (±0.5) mm. The bed was contained in a vessel with internal diameter 27.0 (±0.2) mm and length 100.0 cm. The water was pumped in a closed circuit and controlled by a Bronkhorst Cori-flow mass flow controller; gas flow rate was measured by a rotameter.

The gas and liquid velocities were measured using a spin-echo velocity imaging sequence with ramped phase encode and sinusoidal flow encode gradients to ensure accurate gradient shape. For the 2D gas and liquid velocity measurements of water-SF_6 flow, the gas and liquid superficial velocities were 2.3 and 8.7 $mm\ s^{-1}$, respectively, at 3.7 (±0.1) barg. The velocities of the liquid and gas phases were measured separately on the ^{1}H and ^{19}F channels, respectively. Singly tuned coils were used, and therefore it was necessary to change the r.f. coil without interrupting the flow. During this period, the pressure in the reactor and the superficial velocities of both fluids were kept constant while the outlet pipe from the reactor was temporarily disconnected. To minimise the data acquisition time for the liquid velocity map, the water was doped with Gd^{3+} ions at a concentration of 1.32 mM, giving a spin-lattice relaxation time of 46.5 ms. For the gas velocity imaging, the FOV was 30 mm × 30 mm in a 42 × 42 data array, giving a spatial resolution of 714 μm × 714 μm. The image slice thickness and total data

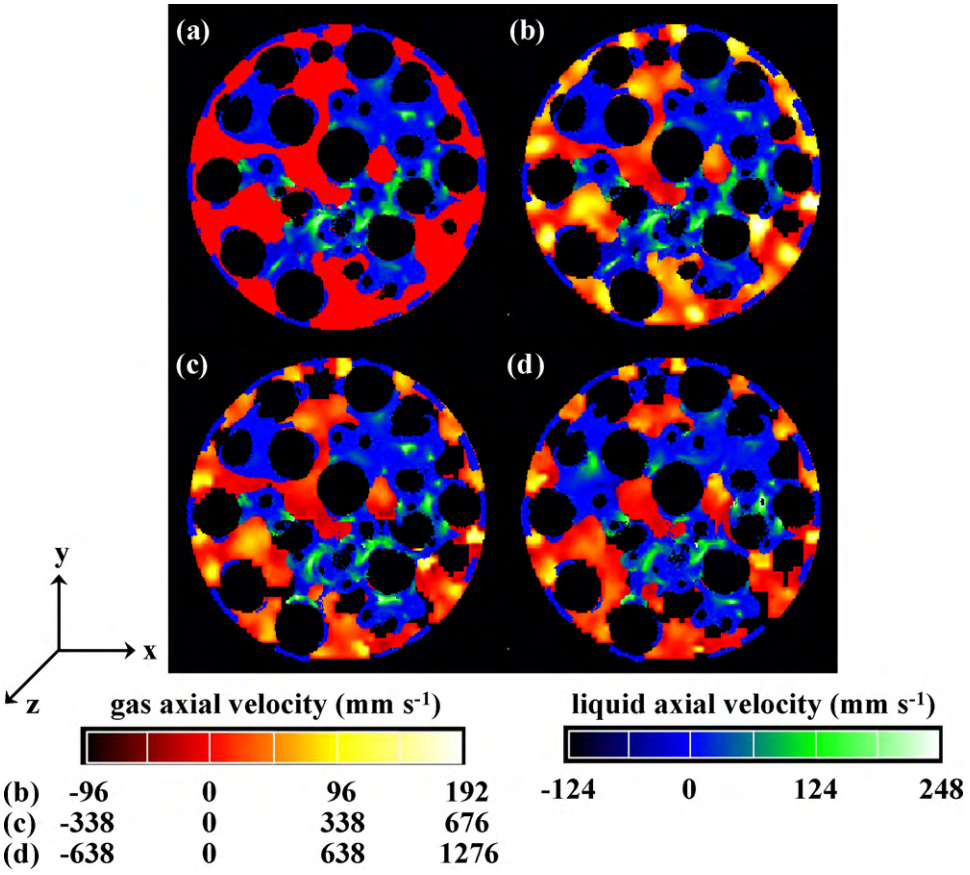

Fig. 3. Magnetic resonance images of gas and liquid velocity fields within a trickle-bed reactor. Gas and liquid velocities are shown by the red-yellow and blue-green colour scales, respectively. In all images the liquid superficial velocity is 2.3 $mm\ s^{-1}$. The gas superficial velocity is (a) 0 $mm\ s^{-1}$, (b) 11.2 $mm\ s^{-1}$, (c) 34.9 $mm\ s^{-1}$ and (d) 61.3 $mm\ s^{-1}$.

acquisition time were 1.5 mm and 22 min, respectively. For the liquid velocity imaging, a field-of-view of 30 mm × 30 mm was used in a 168 × 168 data array, giving a spatial resolution of 179 μm × 179 μm. The image slice thickness and total data acquisition time were 1.5 mm and 10.5 min, respectively.

Fig. 3 shows combined gas–liquid velocity maps. In Fig. 3a there is no gas flow, and the liquid superficial velocity is 2.3 mm s^{-1}. In all images the liquid superficial velocity remains the same and the gas superficial velocity is increased from (b) 11.2 mm s^{-1} to (c) 34.9 mm s^{-1}, through to (d) 61.3 mm s^{-1}. The packing elements within the bed are shown as black (no signal). The location of liquid is indicated by the green-blue colour bar, the particular colour associated with a given pixel indicating the axial liquid velocity at that location. The location of gas is shown by the red-yellow colour bar, and the axial gas velocity indicated by the particular colour on this red-yellow scale. The accuracy of the MRI velocity measurements was confirmed by comparing the total flow rate through the slice section imaged to traditional volumetric measurements of the global flow rate through the bed. Gas and liquid flow rates obtained from the MRI data gave values to within 5 and 7%, respectively of the macroscopic flow rate measurements. From these images some general conclusions may be drawn. For example, the regions of highest gas velocity exist in the centre of local elements of voidage (often referred to as 'pores') between neighbouring packing elements which are predominately gas-filled. The packing elements forming the boundary of these pores tend to be wetted by near-stagnant liquid films. In general, the velocities across a gas–liquid interface are close to zero for both phases, although some regions of high relative (gas–liquid) velocity have been identified. A detailed analysis of these data is ongoing, and will be used to identify the appropriate closure law for use in numerical simulations; e.g. computational fluid dynamics. These measurements also provide direct measurements of gas–liquid and liquid–solid contacting; data which are extremely difficult, if not impossible, to obtain directly using other techniques.

4. Spatial mapping of chemical composition

Previous reports of chemical mapping inside catalytic reactors include ^{1}H MRI [8,9], ^{13}C Distortionless Enhancement by Polarisation Transfer (DEPT) MRI [10,11], and mechanistic studies of catalytic processes using parahydrogen techniques [22]. In terms of quantitative chemical mapping such that accurate composition measurements can be made within the reactor, ^{13}C DEPT measurements probably hold most promise. However, there exist challenges to making accurate measurements. First, although the differing polarisation enhancement of the spectral resonances associated with different CH_n groups can be corrected for using standard procedures [11], the intensities of different spectral peaks are often further influenced as a result of modified spin-lattice and spin–spin relaxation times of the different CH_n groups upon adsorption on to the catalyst surface. Second, analysis of the spectra is further complicated by signal arising from both inside (intra-pellet) and outside (inter-pellet) the catalyst pellets. The reduced spin–spin relaxation time of the chemical species inside the catalyst pellets causes line broadening of each spectral resonance. In ongoing experiments we are now using a partial least-squares algorithm [23] to account for these effects in the data analysis thereby reducing the error in the determinations of chemical compositions obtained. In the partial least-squares approach two variable sets are acquired: an independent *X* variable set made up of ^{13}C DEPT NMR spectra, and a dependent *Y* variable set made up of the calibration concentration measurements. The PLS algorithm iteratively extracts *scores* and *loadings* from the *X* and *Y* datasets that represent linearly independent components from each set. The scores are estimates of the components, or latent-variables, causing the changes in the *X* and *Y* variable sets. The loadings provide a measure of the extent to which each component is expressed in *X* and *Y*. A regression is performed between the extracted scores and loadings of the *X* and *Y* matrices to form the PLS model. In the prediction step, an independent set of ^{13}C DEPT NMR spectra (x_i) are measured from samples of unknown concentration. The PLS model is then used to predict the corresponding sample concentrations (y_i) from the measured x_i. At the superficial liquid flow rates used in this study, the liquid hold-up is such that the population of liquid external to the catalyst pellets accounts for less than 5 mol% of the total liquid within the bed. At these low contents of inter-pellet liquid, the error in determination of the composition of liquid external to the catalyst pellets was deemed unacceptably high at >15 mol%. For this reason only intra-pellet composition measurements have been reported. Errors in the intra-pellet measurements are estimated to be less than 2.5 mol%.

Experiments were performed in a trickle-bed of inner diameter 25 mm, loaded to a bed height of 20 mm with 1 wt% Pd/Al_2O_3 trilobe catalyst (diameter 1.2 mm, length 5 ± 2 mm). The catalyst had been reduced in a 20:80 (v/v). % hydrogen:nitrogen gas flow for 1.5 h prior to study. The catalyst was surrounded above and below by 30 mm layers of pure Al_2O_3 trilobes to provide enhanced gas–liquid distribution and support, respectively.

Before commencing reaction studies, a steady state ^{13}C DEPT MRI reference data set for the case of no reaction was collected by flowing 1-octene (99 mol%), co-currently down through the bed with helium gas at 1 barg at superficial flow rates of 0.06 and 11 mm s^{-1}, respectively. The ^{13}C DEPT chemical shift images showed no significant isomerisation or hydrogenation of 1-octene over the catalyst in the absence of hydrogen. Following this, the liquid flow was maintained at 0.06 ± 0.003 mm s^{-1} and the co-current gas feed of 20:80 (v/v%) hydrogen/nitrogen mixture was introduced, at a pressure of 1 barg for a range of gas flow rates (1.25–14 ± 1 mm s^{-1}). These superficial flow rate measurements correspond to a range of 1-octene:hydrogen molar ratios of 13.5–2.0, respectively; at lower ratios significant vaporization occurred and therefore molar feed ratios below 2.0 were not considered. The reactants were introduced at ambient temperature (20 °C) and air was passed over the reactor to prevent over-heating of the r.f. coil. Only the data for a 1-octene:hydrogen molar ratio of 2 is reported here. RARE images, similar to those recorded in the temperature mapping study described earlier, were used to monitor liquid distribution and confirmed that no significant vaporization occurred during the experiments. The system was monitored as it moved to steady state, typically over a period of 2.5 h. Once steady state had been achieved, ^{13}C DEPT MRI data were acquired with a data acquisition time of 1 h. All outlet samples were analyzed on an Agilent Technologies GC-6890N gas chromatograph using a J&W Scientific HP-5 capillary column with dimensions 30 m × 0.32 mm (inner diameter), and film thickness of 0.25 μm.

The 1D ^{13}C DEPT MRI pulse sequence used is the same as that implemented in our earlier work [11]. A Bruker mini 0.5 probe was combined with a 38 mm birdcage r.f. coil dual-tuned to ^{1}H and ^{13}C resonances of 199.70 MHz and 50.22 MHz. The duration of ^{1}H and ^{13}C 90° pulses were 79 and 75 μs, respectively. The phase encoding gradient, applied along the axial (*z*)-direction of the bed, of duration 0.5 ms was ramped in 16 increments to a maximum value of 3.38 G cm^{-1}. The FOV in the axial direction was 55 mm corresponding to a spatial resolution in this direction of 3.4 mm. In summary, 16 spectra were recorded along the length of the bed. The spectra were acquired from cylindrical volume elements of side length 3.4 mm in the *z*-direction, the data being averaged in the *x*–*y* plane. The location at which the spectra were acquired along the bed is assigned to the mid-point of each volume element. The position of the interface between the pure alumina and

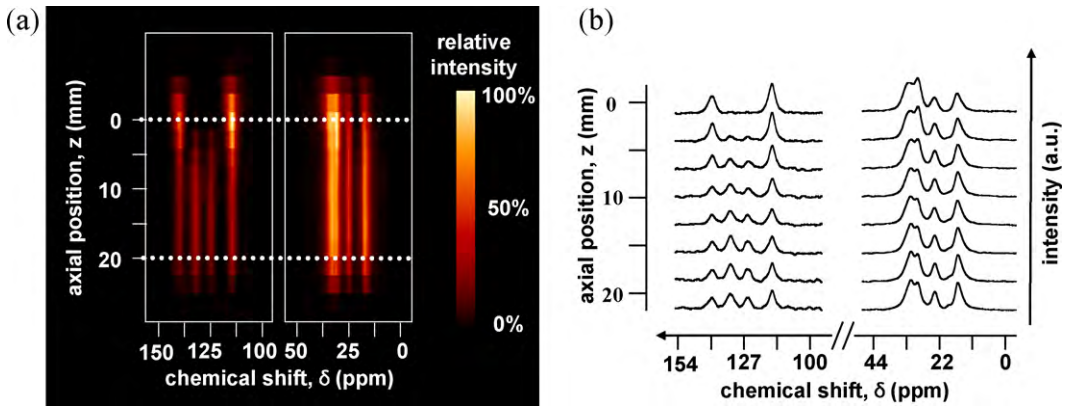

Fig. 4. (a) 2D map of ^{13}C DEPT MRI spectra recorded along the length of the trickle-bed. Separate acquisitions were made for each of the unsaturated and saturated carbon regions of the spectrum. The two horizontal dotted lines indicate the limits of the catalyst packing. (b) Spectra recorded at 8 positions down the bed. Separate spectra are shown for the unsaturated and saturated regions of the ^{13}C DEPT spectrum.

catalyst particles at the top of the bed is identified as $z = 0$ mm. Increasing z-values indicate the direction of superficial flow. Chemical shifts are quoted with reference to the ^{13}C resonance of tetramethylsilane (TMS). Signals were acquired on the carbon channel with a dwell time of 40 μs and a spectral resolution of 0.24 ppm, in the presence of proton decoupling. The unsaturated and saturated regions of the ^{13}C spectrum were acquired separately to ensure efficient DEPT enhancement.

For the measurements made of unsteady state operation during start-up, 16 signal-averages were employed on each region of the carbon spectrum corresponding to a total acquisition time of 15 min. These transient measurements were assigned to the temporal mid-point between the start and end of each data acquisition. Steady state measurements were recorded using 64 signal-averages on each spectral region in a total acquisition time of 1 h. A greater number of signal-averages were used in steady state experiments, where time resolution was not considered critical, in order to maximize signal-to-noise (typically 60–120) and thereby aid determination of composition from the ^{13}C DEPT MRI datasets.

^{13}C DEPT chemical shift images for the case of steady state reaction at a molar ratio of 2.0 are shown in Fig. 4. 2D maps of the ^{13}C DEPT chemical shift datasets, such as Fig. 4a, can be used to assess qualitatively the extent of reaction during the experiment. Any horizontal profile through the 2D map recovers the ^{13}C DEPT spectrum acquired at that location (Fig. 4b). The intensities shown in the 2D map are those of the spectral peaks in the ^{13}C DEPT spectrum. With reference to Fig. 4a, at $z = 0$, at the entrance to the catalyst bed, we see only two peaks occurring in the unsaturated carbon region of the spectrum; these occur at 114 and 139 ppm with respect to TMS and are associated with 1-octene. No other peaks are seen at this position in the bed because no reaction has occurred at this point. As the reactants move down the bed additional peaks are seen at 124 and 131 ppm indicating the formation of 2-octenes. By considering the individual spectral lineshapes (Fig. 4b) it is possible to see evidence of n-octane formation from the subtle changes in the shape and relative intensities of peaks in the saturated ^{13}C spectrum as we move down the bed.

These data can be acquired sufficiently fast that the spatially resolved composition in the bed can be followed in unsteady state systems. In Fig. 5 the mole fractions of 1-octene, 2-octene and n-octane (obtained from PLS analysis of the data shown in Fig. 4) along the length of the reactor are shown at two time points: at 22.5 and 180 min after introduction of hydrogen. The time associated with a given dataset is the time at the half-way point through the total data acquisition time. From these data the conversion and selectivity to 2-octene and n-octane, as a function of both time and axial position along the bed, are obtained. At steady state operation a conversion of 1-octene of ~60% is recorded, as seen from the composition measurement at the end of the reaction zone at $z = 20$ mm.

The ability to measure local composition within a trickle-bed reactor provides the opportunity to study both catalyst and reactor performance on a local scale for the first time. Previous experimental studies of reactions occurring in trickle-beds have been confined to measurement of global reaction rates (e.g. [24–26]). The local composition measurements reported here enable calculations of rate and selectivity to be made on a local scale. The local apparent rate of reaction may be calculated from Eq. (2):

$$r_{\text{app}} = u_{\text{L}} \frac{dC_i}{dz} \tag{2}$$

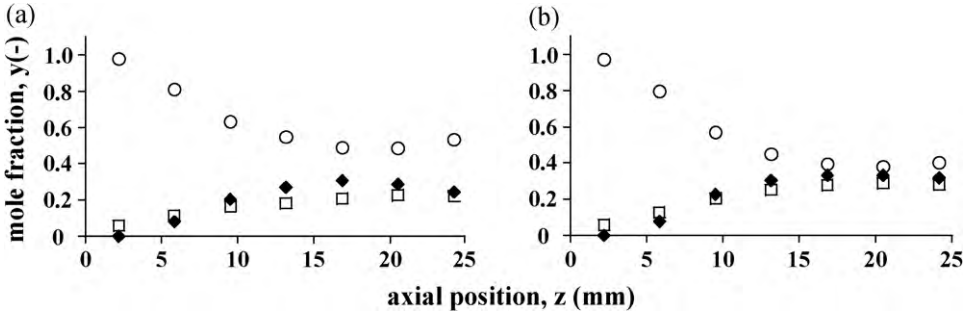

Fig. 5. Time resolved axial composition profiles obtained from ^{13}C DEPT MRI measurements during start-up of the hydrogenation of 1-octene over a fixed-bed of 1 wt% Pd/Al_2O_3 catalyst, for a 1-octene:hydrogen mole ratio of 2.0. Concentrations of 1-octene (○), 2-octene (□), and n-octane (◆) along the length of the bed are shown (a) 22.5 min and (b) 180 min after start-up. Each set of axial profiles at a given time takes 15 min to acquire. The time stated is the mid-point of the acquisition.

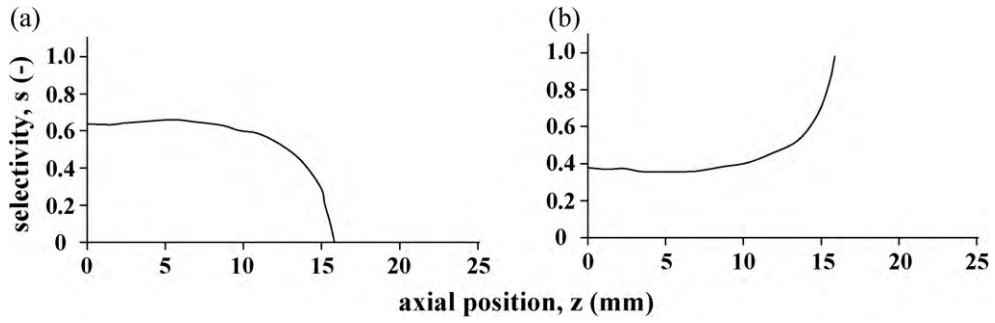

Fig. 6. Local rate-based selectivity measurements obtained from steady state data of the form shown in Fig. 5. (a) Selectivity to n-octane. (b) Selectivity to 2-octenes.

where r_{app} is the apparent reaction rate, u_L is the superficial liquid velocity, C_i is the liquid concentration of species i, and z is the axial distance from the start of the reaction zone. Eq. (2) is obtained from a simplified pseudo-homogeneous reaction model [1], in which the liquid is assumed to move in plug flow through the reactor under conditions of perfect radial mixing. In the absence of data which would allow a more complex model to be adopted, the assumption of a pseudo-homogeneous reactor model provides a simple, transparent means by which to demonstrate how ^{13}C DEPT MRI measurements may be used to generate measurements of local reaction rate.

The ^{13}C DEPT MRI measurements of local composition also allow measurement of local variations in selectivity along the trickle-bed. When composition measurements are available on a local scale, as is the case in these studies, it is most appropriate to define selectivity in terms of the local rate data [27]:

$$s_i(z) = \frac{r_i(z)}{\sum_i^N r_i(z)} \quad (3)$$

where $s_i(z)$ is the selectivity to the product species i, N is the total number of product species formed, and $r_i(z)$ is the local rate of formation of the product species i at axial position z. It is, of course, more usual for selectivity to be defined in terms of composition ratio. However, the concentration at a given point in the bed is dependent on the history of the fluid at each location in the bed and is therefore not a local measurement. Defining the selectivity according to Eq. (3) overcomes this problem and gives a true measure of local selectivity. More detailed discussion of this point, illustrated with comparison of concentration-based and rate-based selectivity data will be reported elsewhere. Fig. 6 shows such data for the bed again operating at a molar ratio of 2, and at steady state. Under these operating conditions, the bed is operating hydrogen lean and this is reflected in Fig. 6 where we see that at ~15 mm into the bed the selectivity to n-octane drops rapidly and the selectivity switches to the isomerisation reaction as the hydrogen becomes depleted. These data are also consistent with the data shown in Fig. 4, where a substantial amount of isomerisation is observed as opposed to immediate full hydrogenation through to the alkane.

5. Conclusions

MRI is particularly well-suited to *operando* studies of catalytic processes. Here we demonstrate its ability to map temperature, gas and liquid velocity fields, and chemical composition. The accuracy of each of these types of measurements has been addressed. Temperature mapping is accurate to ±2.0 °C. Images of local gas and liquid flow velocities are shown to provide determinations of gas and liquid flow rate in agreement with traditional 'global' flow rate determinations to within 5 and 7%, respectively. These datasets also provide direct measurements of gas–liquid contact area and catalyst wetting. Partial least-squares analysis of spatially resolved ^{13}C DEPT MRI data give a measurement accuracy of better than 2.5% in the determination of chemical composition within local volume elements within the reactor. Of particular interest is the observation that the measurements of chemical composition also allow calculation of local concentration- and rate-based selectivity data which, when combined with the local measurements of hydrodynamics, will allow us to explore in greater detail than has hitherto been possible, the coupling of hydrodynamics, mass transfer and chemical kinetics in heterogeneous catalytic systems.

Acknowledgements

MHS acknowledges the University of Cambridge and Trinity College, Cambridge for financial support. FJRA acknowledges the FCT (Portuguese Foundation for the Science and Technology) for financial support under the PhD grant SFRH/BD/28548/2006. DJH, AJS, CPD and LFG acknowledge support from EPSRC grants GR/S43719/01, GR/S20789/01 and EP/G011397/1.

References

[1] A. Gianetto, V. Specchia, Chem. Eng. Sci. 47 (1992) 3197.
[2] L.F. Gladden, M.D. Mantle, A.J. Sederman, Adv. Catal. 50 (2006) 1.
[3] L.F. Gladden, AIChE J. 49 (2003) 2.
[4] A.J. Sederman, L.F. Gladden, Chem. Eng. Sci. 56 (2001) 2615.
[5] N.L. Nguyen, V. van Buren, A. von Garnier, E.H. Hardy, R. Reimert, Chem. Eng. Sci. 60 (2005) 6289.
[6] L.F. Gladden, Top. Catal. 24 (2003) 19.
[7] L.D. Anadon, A.J. Sederman, L.F. Gladden, AIChE J. 52 (2006) 1522.
[8] E.H.L. Yuen, A.J. Sederman, L.F. Gladden, Appl. Catal. A 232 (2002) 29.
[9] I.V. Koptyug, A.A. Lysova, A.V. Kulikov, V.A. Kirillov, V.N. Parmon, R.Z. Sagdeev, Appl. Catal. A 267 (2004) 143.
[10] B.S. Akpa, M.D. Mantle, A.J. Sederman, L.F. Gladden, Chem. Commun. (2005) 2741.
[11] A.J. Sederman, M.D. Mantle, C.P. Dunckley, Z.Y. Huang, L.F. Gladden, Catal. Lett. 103 (2005) 1.
[12] W. Wlodarczyk, M. Hentschel, P. Wust, R. Noeske, N. Hosten, H. Rinneberg, R. Felix, Phys. Med. Biol. 44 (1999) 607.
[13] A.V. Koptyug, A.V. Khomichev, A.A. Lysova, R.Z. Sagdeev, J. Am. Chem. Soc. 130 (2008) 10452.
[14] R. Kimmich, D. Hoepfel, J. Magn. Reson. 72 (1987) 379.
[15] C. Ammann, P. Meier, A.E. Merbach, J. Magn. Reson. 46 (1982) 319.
[16] J. Henning, A. Nauerth, H. Friedburg, Magn. Reson. Med. 3 (1986) 823.
[17] A.L. van Geet, Anal. Chem. 40 (1968) 2227.
[18] A.L. van Geet, Anal. Chem. 42 (1970) 679.
[19] O. Yamamoto, M. Yanagisawa, Anal. Chem. 42 (1970) 1463.
[20] A.J. Sederman, L.F. Gladden, AIChE J. 51 (2005) 615.
[21] M.H. Sankey, D.J. Holland, A.J. Sederman, L.F. Gladden, J. Magn. Reson. 196 (2009) 142.
[22] K.V. Kovtunov, I.E. Beck, V.I. Bukhtiyarov, I.V. Koptyug (Eds.), Angew. Chem. Int. 47 (2008) 1492.
[23] P. Geladi, B.R. Kowalski, Anal. Chim. Acta 185 (1986) 1.
[24] B.D. Babcock, G.T. Mejdell, O.A. Hougen, AIChE J. 3 (1957) 366.
[25] M. Banchero, L. Manna, S. Sicardi, J.G. Boelhouwer, M.I. Urseanu, G. Kwant, Chem. Eng. Sci. 59 (2004) 5411.
[26] M. Herskowitz, R.G. Carbonell, J.M. Smith, AIChE J. 25 (1979) 272.
[27] J.J. Carberry, A. Varma, Chemical Reaction and Reactor Engineering, Marcel Dekker, New York, 1987.